Preprints of the 21st IFAC World Congress (Virtual)
Berlin, Germany, July 12-17, 2020

Dual-Stage Control Structure for Multilevel Voltage Source Inverters ⋆

Eduardo G. Nery [*,***] **Guilherme A. Pimentel** [*]
Eduardo R. Rohr [**] **Aurélio T. Salton** [***]

[*] *PUCRS - Group of Automation and Control Systems, Av. Ipiranga 6681, Porto Alegre, Brazil, 90619-900 (e-mail: eduardo.nery@acad.pucrs.br, guilherme.pimentel@pucrs.br)*
[**] *ABB Corporate Research Center Dattwil CH-5405 Baden 5, Switzerland (e-mail: eduardo.rohr@ch.abb.com)*
[***] *UFRGS - Department of Electrical Engineering, Av. Osvaldo Aranha 103, Porto Alegre, Brazil, 90035-190 (e-mail: aurelio.salton@ufrgs.br)*

Abstract:
This work proposes an alternative for total harmonic distortion (THD) attenuation in power inverters by combining two different circuit stages. The Macro stage comprises of a Neutral-Point-Clamped (NPC) multilevel inverter operating in high voltage and low switching frequency. The Micro stage is a two-level three-phase inverter, which is faster and more accurate due to its higher frequency and limited voltage. In this dual-stage approach, the opposite characteristics of the converters lead the Micro stage to correct the distortions of the Macro. It is possible to work with small values of filtering components, lower than the ones needed in a one-stage approach. This way, the presented proposal aims to reduce the physical size of the converter and its costs. The NPC inverter works in open loop with its switching signals generated by optimized pulse patterns (OPP). For correct THD filtering, a resonant control strategy with a Notch filter is designed in the frequency domain, as well as a feedforward structure designed in time domain. Simulation results show that the proposed system keeps voltage THD in acceptable levels for IEEE Standards.

Keywords: Dual-Stage Actuators, Optimized Pulse Patterns, Multilevel Power Converters, Resonant Control, Voltage Source Inverters

1. INTRODUCTION

Static power dc-ac converters, also known as inverters, convert electricity in direct current (dc) into alternate current (ac). The ac output waveforms of these devices are made up of discrete values, since they are generated from switching devices. This discrete feature leads to low efficiency in electric motors and transmission lines (Motapon et al., 2012), for example. Because of that, the output waveforms are smoothed by low-pass inductive-capacitive (LC) filters connected between the inverter output terminals and the load input terminals. However, the conciliation between output signal quality and efficiency usually limits the switching frequency, which leads to high values of total harmonic distortion (THD) that require large and bulky LC filters (Prodanovic and Green, 2003). Also, the filtered output waveform is not a perfect sinusoidal signal because it still has a relatively high ripple, which keeps the system vulnerable to low efficiency, skin effect, overshoot, and power quality degradation (Asadi and Jalilian, 2012).

Control algorithms are usually applied to inverters aiming to minimize the effect of disturbances on the dc input (Errouissi et al., 2016). It is also possible to synchronize the output signal with an ac voltage load, such as an operating motor or the electrical grid (Geyer et al., 2012; Cabral et al., 2016). In (Pérez-Ibacache et al., 2018), the authors apply a linear-quadratic regulator (LQR) controller to ac microgrids. The resonant control is suggested as an improving alternative for THD attenuation in (Mirhosseini et al., 2016), and the authors point out that this strategy may work in the $\alpha\beta$-frame due to its sinusoidal reference. It saves computational cost of working in the dq-frame recommended for proportional-integral (PI) controllers (Ebrahimi et al., 2016).

The Optimized Pulse Patterns (OPP) approach proposes an offline alternative to Pulse Width Modulation (PWM) techniques to generate the inverter switching command signals (Geyer, 2011). In OPP, the switching signals are computed only once. The main issues of working with OPP in closed loop, however, are related to the varying modulation index. It may cause discontinuities which affect linear control systems efficiency (Vasiladiotis et al., 2019). Also, OPP-generated signals present slow equivalent frequency and so, despite the reduction of switching losses, it requires

⋆ This study was financed in part by the Coordenação de Aperfeiçoamento de Pessoal de Nível Superior - Brasil (CAPES) - Finance Code 001.

high-valued LC filters in order to keep the output voltage free of harmonic distortion.

The concept of dual-stage actuators (DSA) applied to power converters may surge as an alternative to reduce THD. It comprises two similar plants with opposite characteristics: the Macro actuator has a long range of actuation, but has a slow response; the Micro actuator is faster and more accurate than the Macro, however, has a limited range of actuation (Salton, 2011). Combining both actuators with adequate control structures may lead the Micro to compensate for the effect of disturbances on the Macro. DSA may be applied to electronic systems such that an electric circuit is designed to compensate some ripple present on the output voltage or current of another circuit. This ripple may be caused by distortions on the dc power supply or on the actuator and load connections, or even by filter residuals.

This paper presents a control strategy for THD attenuation in OPP-operated dc-ac converters with small-valued LC filters. The alternative combines different stages in the same system, as suggested by the DSA approach, with the Macro being a three-level Neutral Point Clamped (3L-NPC) inverter operating in high levels of voltage and current. Its switching signals are generated by OPP in open loop, on an equivalent frequency of some hundreds of hertz, in order to reduce switching losses. Simultaneously, the Micro is a two-level three-phase (2L-3ϕ) inverter connected to the Macro, operating at limited levels of voltage and current and controlled by PWM. The higher switching frequency allows the Micro to attenuate the remaining ripple on the Macro.

In order to operate efficiently, the Micro actuator works in closed loop with a resonant control structure, and also in open loop with a feedforward controller. The latter one is designed based on a model of the harmonic distortion present on the NPC inverter output voltage. First-principles models of the connection between both the Macro and the Micro LC filters are defined for frequency response analysis, from which the resonant control is designed.

2. PRELIMINARIES

The main theoretical concepts about OPP, DSA, and the theory of feedforward and resonant controllers are described in the following.

2.1 Optimized Pulse Patterns

The OPP method defines a set of switching angles $\mathbf{\Theta}$, which represents the instants when the switches change its states over a period of operation. It also defines a vector of voltage transitions $\mathbf{f}$, which states whether the switches may open or close at each instant of $\mathbf{\Theta}$. It is possible to describe the output phase voltage of a 3L-NPC inverter, $\mathbf{v}_n(t) = [v_{a_n}(t)\ v_{b_n}(t)\ v_{c_n}(t)]^\mathsf{T}$, as Fourier series from $\mathbf{\Theta}$ and $\mathbf{f}$:

$$\begin{aligned} \mathbf{v}_n(t) &= \sum_{h=1}^{\infty} V_h \sin\left(h\theta + \mathbf{\Phi}\right), \\ V_h &= \frac{4}{h\pi} \sum_{k=1}^{K} f_k \cos\left(h\theta_k\right),\ h = 1, 3, 5, \ldots, \infty, \end{aligned} \tag{1}$$

where $\theta = \omega t$, $0 \leq \theta \leq \pi/2$. K represents the number of voltage transitions over a quarter of period (the number of elements in $\mathbf{\Theta}$ and $\mathbf{f}$), $f_k \in \mathbf{f}$ and $\theta_k \in \mathbf{\Theta}$, $0 < \theta_k < \pi/2$ represent the k-th element of $\mathbf{f}$ and $\mathbf{\Theta}$, respectively. V_h represents the amplitude of the harmonic contents, and $\mathbf{\Phi} = [0\ -2\pi/3\ -4\pi/3]^\mathsf{T}$ rad is the phase delay of each voltage waveform of $\mathbf{v}_n(t)$. Even-order harmonics are considered as equal to zero, due to the half-wave symmetry.

The sets $\mathbf{\Theta}$ and $\mathbf{f}$ are calculated based on a selected objective function $J(\theta)$ which must be minimized. This work aims to reduce voltage THD in multilevel inverters output. The percentage of THD is computed as:

$$\text{THD}\ (\%) = \frac{\sqrt{{V_2}^2 + {V_3}^2 + {V_4}^2 + \ldots + {V_\infty}^2}}{V_1} \times 100,$$

where V_i represents the amplitude of the i-th harmonics, and V_1 is the fundamental frequency amplitude.

So, in order to simplify the optimization algorithm, $J(\theta)$ is defined as the sum of even order harmonics:

$$J(\theta) = \sum_{h \in \mathcal{H}} {V_h}^2,\ \mathcal{H} := \{3, 5, 7, \ldots, \infty\}$$

2.2 Dual-Stage Actuators

The concept of dual-stage actuators (DSA), or macro-micro systems, comprises two similar plants with opposite characteristics. The main stage actuator, or the Macro, has a long range of actuation. However, it also has a slow response and it is susceptible to disturbances. The fine stage, also called auxiliary or Micro actuator, is faster and more accurate than the Macro, but it has a limited range of actuation. The DSA approach suggests combining both actuators such that the Micro compensates the effect of disturbances on the Macro.

There are several dual-stage control structures (Salton, 2011). On the decoupled control structure illustrated in Fig. 1, the actuation is centered on the Micro stage: the Macro controller $G_{c_1}(s)$ is only required to generate a coarse tracking – possibly working in open loop – because the remaining error is compensated via feedback by the Micro actuator loop. It is possible to define

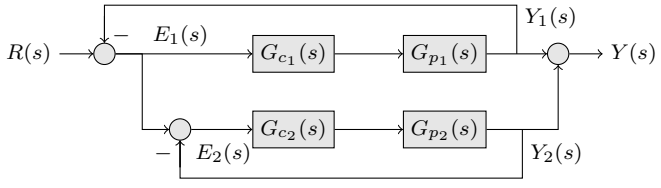

Fig. 1. Decoupled feedback dual-stage control structure (Adapted from Salton (2011)).

the Micro actuator error $E_2(s)$ as the difference between the reference $R(s)$ and the system output $Y(s)$. Since

$Y(s) = Y_1(s) + Y_2(s)$, in order to $Y(s)$ to follow the reference $R(s)$, $Y_2(s)$ must follow $E_1(s)$.

$$E_1(s) = R(s) - Y_1(s),$$
$$E_2(s) = E_1(s) - Y_2(s),$$
$$E_2(s) = R(s) - Y_1(s) - Y_2(s) = R(s) - Y(s).$$

2.3 Feedforward Controller

Feedforward systems control the plant input predicting the disturbance effect on the output. Compared to feedback systems, the main advantages of working with feedforward controllers are related to the faster response and the fact that there is no need of measurements. However, they work on open loop, and consequently, do not correct errors caused by unpredicted disturbances or model uncertainties. The block diagram shown in Fig. 2 represents an example of a feedforward control structure whose inputs are the reference and a known disturbance $D(s)$. In the

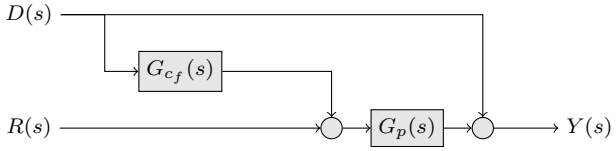

Fig. 2. Disturbance controlled feedforward stucture.

structure shown in Fig. 2, $G_p(s)$ represents the transfer function of the plant. The feedforward controller $G_{c_f}(s)$ manipulates the plant input in order to reduce the effect of the predicted disturbance. In the context of this work, a feedforward structure similar to the one shown in Fig. 2 may model the error between the reference and the NPC inverter output, and control the Micro actuator such that it operates on the predicted error.

2.4 Resonant Controllers and Internal Model Principle

The Internal Model Principle (IMP) is a theoretical concept of control system design for periodical reference tracking. Since the remaining error to be tracked by the 2L-3ϕ inverter presents sinusoidal harmonic behaviour, the IMP applied in the form of a resonant controller may achieve better reference tracking (Castro et al., 2014; de Oliveira et al., 2018).

The resonant controller inserts a sinusoidal dynamics in the system determined by the frequency ω_r.

$$G_{c_r}(s) = \frac{U(s)}{E(s)} = \frac{\omega_r^2}{s^2 + \omega_r^2}, \tag{2}$$

where $U(s)$ represents the controller output behaviour and the plant input, and $E(s)$, the reference-to-output system error and the controller input.

The main feature of the control structure in (2) is the infinite gain on ω_r, due to the pair of imaginary poles located in $s = \pm j\omega_r$. Expanding (2) to H harmonics to be attenuated, and adding a pair of complex zeros in order to avoid stability issues, the multiple-resonant control structure results in (Pereira et al., 2014):

$$G_{c_r}(s) = \sum_{i=1}^{H} \left(K_{r_i} \frac{s^2 + 2\xi_{r_i}\omega_{r_i} + \omega_{r_i}^2}{s^2 + \omega_{r_i}^2} \right). \tag{3}$$

The gains K_{r_i}, as well as the damping factors ξ_r and the frequencies ω_{r_i}, may be determined graphically from the frequency spectrum of the signal to be tracked.

The LC filter of the Micro stage, however, may amplify high frequency harmonics in the system output. An alternative to prevent the Micro actuator from working on these frequencies is by means of a Notch filter:

$$G_{c_n} = K_n \frac{s^2 + \omega_n^2}{s^2 + 2\xi_n\omega_n + \omega_n^2}, \tag{4}$$

where ω_n is the angular frequency of the harmonic contents to be attenuated from the output signal.

The addition of the Notch filter to $G_{c_r}(s)$ is similar to the multiple-resonant control structure defined in (3). Considering H harmonics to be attenuated:

$$G_{c_r}(s) = \sum_{i=1}^{H} \left(K_{r_i} \frac{s^2 + 2\xi_{r_i}\omega_{r_i} + \omega_{r_i}^2}{s^2 + \omega_{r_i}^2} \right) + K_n \frac{s^2 + \omega_n^2}{s^2 + 2\xi_n\omega_n s + \omega_n^2}. \tag{5}$$

3. MATHEMATICAL MODEL

This section defines a mathematical model of the dual-stage LC filter in order to obtain its response related to each actuator individually. It is also presented the open loop analysis of the Macro converter operating disconnected from the Micro.

3.1 Dual-Stage LC Filter

The circuit seen in Fig. 3 represents a single-phase schematic model of the connection between the LC filters. L_1 and C_1 represent the filtering components of the Macro stage, whereas L_2 and C_2 represent the same for the Micro stage, and Z is the load equivalent impedance. The filter inputs, $u_{L_1}(t)$ and $u_{L_2}(t)$, are the output signals from the 3L-NPC inverter and the 2L-3ϕ inverter, respectively. Since the filter model is a multiple-input-multiple-output

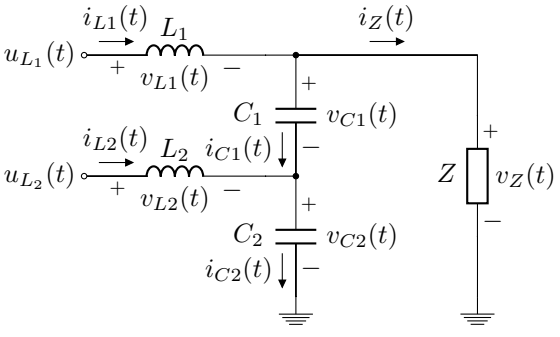

Fig. 3. Single-phase model of the dual-stage LC filter.

system, a matrix of transfer functions that describes the response for each input and output of the dual-stage LC system is defined as:

$$\begin{bmatrix} V_{C1}(s) \\ V_{C2}(s) \end{bmatrix} = \begin{bmatrix} G_{11}(s) & G_{12}(s) \\ G_{21}(s) & G_{22}(s) \end{bmatrix} \begin{bmatrix} U_{L_1}(s) \\ U_{L_2}(s) \end{bmatrix}$$
$$= \frac{1}{\Delta(s)} \begin{bmatrix} ZL_2C_2s^2 + Z & -(L_1s + Z) \\ ZC_1L_2s^2 & ZL_1C_1s^2 + L_1s + Z \end{bmatrix} \begin{bmatrix} U_{L_1}(s) \\ U_{L_2}(s) \end{bmatrix},$$

where $\Delta(s) = ZL_1C_1L_2C_2s^4 + L_1L_2(C_1 + C_2)s^3 + Z(L_1C_1 + C_1L_2 + L_2C_2)s^2 + L_1s + Z$.

From the capacitor series connections, the load voltage $v_Z(t)$ is equal to the sum of the voltage across the capacitors ($v_Z(t) = v_{C1}(t) + v_{C2}(t)$). So, the Macro stage load voltage transfer function $G_{p_1}(s)$ is defined as the sum of $G_{11}(s)$ and $G_{21}(s)$. Similarly, the Micro stage transfer function $G_{p_2}(s)$ is the sum of $G_{12}(s)$ and $G_{22}(s)$.

$$G_{p_1}(s) = \frac{V_Z(s)}{U_{L_1}(s)} = \frac{ZL_2(C_1+C_2)s^2 + Z}{\Delta(s)}$$
$$G_{p_2}(s) = \frac{V_Z(s)}{U_{L_2}(s)} = \frac{ZL_1C_1s^2}{\Delta(s)}$$

3.2 Design Parameters

As stated before, the Macro converter operates in high levels of voltage and current and slow switching frequency. To smooth the output waveform efficiently, an adequate LC filter presents large capacitance and inductance. Doing so results in a bulky and more expensive circuit. Table 1 lists the parameters of the Macro actuator. The designed components are more feasible, but the cut-off frequency of the filter (f_{c_1}) is greater than required. So, it is expected high THD caused by low frequency harmonics.

Table 1. Macro actuator parameters

Parameter	Value
DC input voltage (V_{dc_1})	3000 V
OPP switching frequency (f_{s_1})	350 Hz
Filter inductance ($L_{1_{a,b,c}}$)	400 µH
Filter capacitance ($C_{1_{a,b,c}}$)	63 µF

The cut-off frequency of the Macro LC filter is set as:

$$f_{c_1} = \frac{1}{\sqrt{L_1C_1}} = 6300\,\text{rad/s} \approx 1000\,\text{Hz}. \quad (6)$$

The capacitance of the Micro stage LC filter follows the relation between the dc inputs of the inverters. Meanwhile, the inductance was defined such that the cut-off frequency of the Micro LC filter is ten times bigger than the Macro. The higher switching frequency and lower operation voltage make the Micro stage faster than the Macro. The filter, however, may amplify some high-order harmonics. Table 2 lists the parameters of the Micro actuator. The cut-off

Table 2. Micro actuator parameters

Parameter	Value
DC input voltage (V_{dc_2})	600 V
PWM switching frequency (f_{s_2})	20 kHz
Filter inductance ($L_{2_{a,b,c}}$)	20 µH
Filter capacitance ($C_{2_{a,b,c}}$)	12.6 µF

frequency of the Micro LC filter is:

$$f_{c_2} = \frac{1}{\sqrt{L_2C_2}} = 63\,000\,\text{rad/s} \approx 10\,000\,\text{Hz} \quad (7)$$

The load is set as a three-phase ac line voltage source of 1470 V, 50 Hz with 1 Ω series resistance and 31.8 mH series inductance. The reference $\mathbf{r}(t) = [r_a(t)\ r_b(t)\ r_c(t)]^\mathsf{T}$ is given as a three-phase 3000 V_{pp} ac voltage waveform with 50 Hz frequency.

3.3 Macro Actuator Analysis

The 3L-NPC inverter switching signals are generated offline by OPP. The sets $\mathbf{\Theta}$ and $\mathbf{f}$ are defined as:

$$\mathbf{\Theta} \simeq \left[\ 19^\circ\ 44^\circ\ 50^\circ\ 55^\circ\ 59^\circ\ 79^\circ\ 89^\circ\ \right]^\mathsf{T},$$
$$\mathbf{f} = \left[\ \ 1\ -1\ \ 1\ -1\ \ 1\ -1\ \ 1\ \right]^\mathsf{T}.$$

Due to quarter-wave symmetry, the remaining switch angles and voltage transitions are defined by reflections over 90°. Fig. 4 presents the phase a waveform of the 3L-NPC inverter control input $\mathbf{u}_1(t)$. The same signal applies to phases b and c respecting their phase delays.

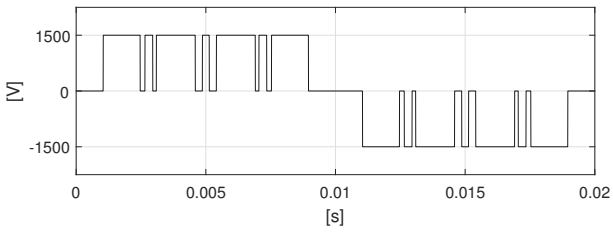

Fig. 4. Macro actuator control signal waveform: $u_{1_a}(t)$.

In a first moment, the Macro actuator is simulated disconnected from the Micro, in order to obtain the 3L-NPC inverter response for the given parameters. In this scenario, the three-phase system is implemented in MATLAB/Simulink environment throughout the Simscape package such as the schematics shown in Fig. 5. The

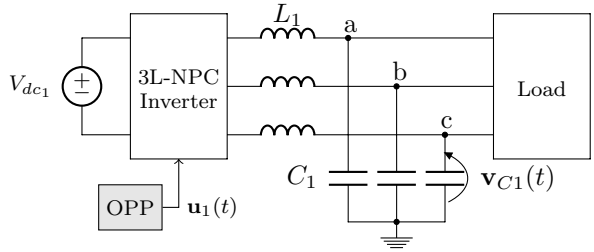

Fig. 5. Decoupled Macro actuator schematic circuit.

waveforms of $\mathbf{v}_{C1}(t) = [v_{C1_a}(t)\ v_{C1_b}(t)\ v_{C1_c}(t)]^\mathsf{T}$ obtained from the described simulation in steady state are depicted in Fig. 6, as well as their frequency spectrum. The distortion seen in the waveforms of (a) is mainly caused by the LC filters, since the resonance peak around 1 kHz observed on the frequency spectrum of (b) corresponds to the value of f_{c_1} computed in (6). It is also noticed the fundamental frequency (V_1) in 50 Hz.

4. CONTROL SYSTEM DESIGN

The proposed system applies the DSA concept to dc-ac converters for load voltage THD attenuation. The output of the 2L-3ϕ inverter is controlled accordingly to the error between the reference and the 3L-NPC inverter output. Therefore, it is possible to reduce THD on the load voltage with small and feasible LC filters. The connection of both inverters is schematically represented in Fig. 7. The figure also presents the block diagram of the proposed dual-stage control structure, which combines the structures shown in Fig. 1 and Fig. 2.

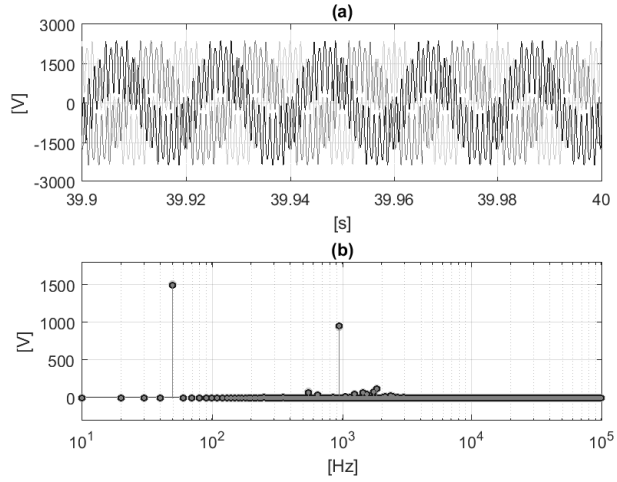

Fig. 6. Waveforms (a) and frequency spectrum (b) of $\mathbf{v}_{C1}(t)$ with the Macro disconnected from the Micro.

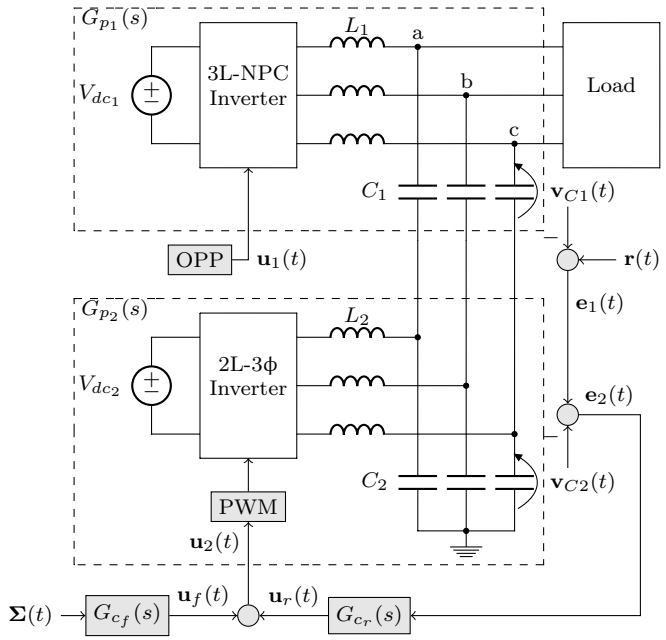

Fig. 7. Proposed dual-stage structure.

4.1 Feedforward Controller Design

The feedforward control is based on model inversion and relies on the fact that the error generated by the OPP is known from (1). Let $\Sigma(t)$ represent the undesired higher harmonics of (1), then, the feedforward controller $G_{c_f}(s)$ is designed as a transfer function that obtains $U_f(s)$ from $R(s)$ and $\Sigma(s)$ as follows:

$$U_f(s) = \frac{\Delta(s)R(s)}{ZL_1C_1s^2 + L_1s + Z} \cdots \\ \cdots - \frac{\Delta(s)\Sigma(s)}{ZL_1{}^2C_1{}^2s^4 + L_1{}^2C_1s^3 + ZL_1C_1s^2}. \tag{8}$$

In steady state, the feedforward control input $\mathbf{u}_f(t)$ is readily given as the following expression, where ω_0 is the fundamental frequency:

$$\mathbf{u}_f(t) = \frac{1}{\sqrt{3}} \sum_{h=3}^{99} V_h \Big\{ \sin\Big[\omega_0 ht + \mathbf{\Phi} + \underline{\angle G_{c_f}(j\omega_0 h)}\Big] - \dots \\ \dots - \sin\Big[\omega_0 ht - 2\pi/3 + \mathbf{\Phi} + \underline{\angle G_{c_f}(j\omega_0 h)}\Big]\Big\} \Big| G_{c_f}(j\omega_0 h) \Big|.$$

4.2 Resonant Controller Design

With the feedforward controller, it is expected that only the harmonics amplified by the dual-stage LC filter remain on the output signal. As computed in (6) and (7), these harmonics are close to 1 kHz and 10 kHz.

The first harmonic is seen as a disturbance from the Micro inverter. Therefore, it is compensated by a resonant controller designed as in (2) for $\omega_{r_1} = 2\pi\,950\,\text{rad/s}$, $\xi_{r_1} = 0.01$ and $K_{r_1} = 0.1$. In order to compensate the resonant peak due to L_2C_2, the Notch filter structure, presented in (4), is employed with $\omega_n = 2\,\pi 10\,250\,\text{rad/s}$, $\xi_n = 2$ and $K_n = 1$. In addition, two more resonant controllers, with respect to the multiple-resonant structure presented in (3), are designed to attenuate some remaining harmonics observed from simulations of the resonant structure. These harmonics are of $\omega_{r_2} = 2\pi\,550\,\text{rad/s}$ and $\omega_{r_3} = 2\pi\,650\,\text{rad/s}$, with the same gains and dumping factors as the previously defined controller.

The designed controller introduces peaks on the low frequency harmonics, and a valley around 10 kHz which attenuates the correspondig peak, as illustrated in Fig. 8.

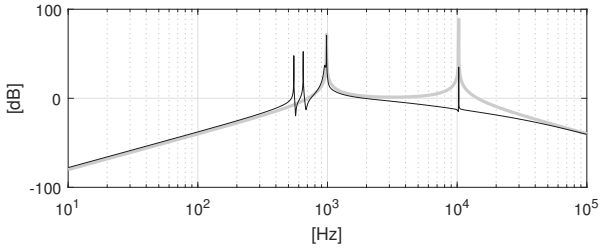

Fig. 8. Magnitude of $G_{p_2}(s)$ (light) and $G_{p_2}(s)G_{c_r}(s)$ (dark) Bode Diagrams.

4.3 Numerical Results

The circuit and the control structure shown in Fig. 7 are implemented in MATLAB/Simulink environment according to the parameters presented in Tables 1 and 2. The proposed dual-stage control structure effectively reduced the harmonic content in steady-state, smoothing the output waveforms as depicted on Fig. 9. The structure comprised of feedforward controller and the multiple-resonant and Notch filter controllers successfully keep the system operating in acceptable THD values according to IEEE Standards (IEEE, 2014), which states that voltage THD of inverters operating between 1 kV and 69 kV must not trespass 5 %. Table 3 compares the obtained voltage THD for each scenario presented on this paper.

5. CONCLUSION

This work suggests a new approach to optimize multilevel inverters modulated by OPP avoiding bulky LC filters. A

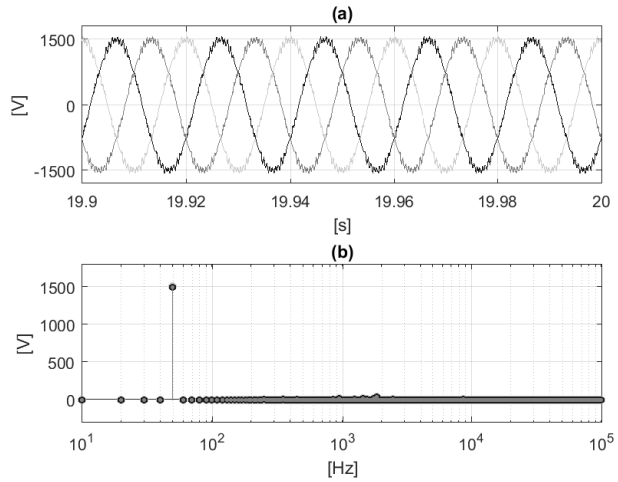

Fig. 9. Waveforms (a) and frequency spectrum (b) of $\mathbf{v}_Z(t)$ with the designed dual-stage control structure.

Table 3. Comparison of numeric results obtained with the presented structures.

Control System	Phase	THD (%)	Error (%)
Macro Actuator	*a*	65.1	0.41
	b	65.1	0.41
	c	64.6	0.41
Dual-stage Control	*a*	3.98	0.02
	b	3.98	0.02
	c	3.98	0.02

two-level three-phase inverter is connected to a multilevel NPC inverter though the filtering components, based on the theory of dual-stage actuators. The proposed control system is composed of a feedforward controller designed from a mathematical model of the disturbance on the NPC inverter output voltage. From the open loop analysis and models of the dual-stage LC filter behaviour, a multiple-resonant controller with a Notch filter was designed to reject harmonics that end up enhanced by the filter. Simulation results validated the obtained models and proved that the feedforward and the multiple-resonant controllers kept the output voltage THD in acceptable levels.

ACKNOWLEDGEMENTS

The authors acknowledge the financial support of CAPES and CNPq, Brazil, under grant 306214/2018-0, and the technical contribution of ABB Switzerland Ltd.

REFERENCES

Asadi, M. and Jalilian, A. (2012). Three-level NPC inverter control system of hybrid active power filter by modulation ratios of switching functions. In *2012 Proceedings of 17th Conference on Electrical Power Distribution*, 1–8. IEEE.

Cabral, H.G., Guisso, I.L., de Faria, P.F., Rambo, C.E., dos Reis, F.B., Vieira, Jr., V.A., Nery, E.G., Viero, R.C., Pan, A.C., and dos Reis, F.S. (2016). A micro inverter based on Ćuk converter for PV modules with anti-islanding and MPPT schemes. In *12th IEEE International Conference on Industry Applications*, 1–8.

Castro, R.d.S., Flores, J.V., Salton, A.T., and Pereira, L.F.A. (2014). A comparative analysis of repetitive and resonant controllers to a servo-vision ball and plate system. *IFAC Proceedings Volumes*, 47(3), 1120–1125.

de Oliveira, M.S., Salton, A.T., Flores, J.V., and Pimentel, G.A. (2018). Resonant gain scheduling controller for spiral scanning patterns in atomic force microscopy. In *Intelligent Robotics and Applications*, 255–267. Springer International Publishing.

Ebrahimi, M., Khajehoddin, S.A., and Karimi-Ghartemani, M. (2016). Fast and robust single-phase *DQ* current controller for smart inverter applications. *IEEE Transactions on Power Electronics*, 31(5), 3968–3976.

Errouissi, R., Al-Durra, A., and Muyeen, S. (2016). Design and implementation of a nonlinear pi predictive controller for a grid-tied photovoltaic inverter. *IEEE Transactions on Industrial Electronics*, 64(2), 1241–1250.

Geyer, T. (2011). A comparison of control and modulation schemes for medium-voltage drives: Emerging predictive control concepts versus PWM-based schemes. *IEEE Transactions on Industry Applications*, 47(3), 1380–1389.

Geyer, T., Oikonomou, N., Papafotiou, G., and Kieferndorf, F.D. (2012). Model predictive pulse pattern control. *IEEE Transactions on Industry Applications*, 48(2), 663–676.

IEEE (2014). IEEE recommended practice and requirements for harmonic control in electric power systems. *IEEE Std 519-2014 (Revision of IEEE Std 519-1992)*, 1–29. doi:10.1109/IEEESTD.2014.6826459.

Mirhosseini, M., Pou, J., Karanayil, B., and Agelidis, V.G. (2016). Resonant versus conventional controllers in grid-connected photovoltaic power plants under unbalanced grid voltages. *IEEE Transactions on Sustainable Energy*, 7(3), 1124–1132.

Motapon, S.N., Arnedo, L., Mashal, H., and Patke, A. (2012). Hybrid damping of grid-tie inverter output harmonics for resonance rejection and wind park stability under high penetration. In *2012 IEEE Power Electronics and Machines in Wind Applications*, 1–4.

Pereira, L.F.A., Flores, J.V., Bonan, G., Coutinho, D.F., and da Silva, J.M.G. (2014). Multiple resonant controllers for uninterruptible power supplies — a systematic robust control design approach. *IEEE Transactions on Industrial Electronics*, 61(3), 1528–1538.

Pérez-Ibacache, R., Silva, C., and Yazdani, A. (2018). Linear state-feedback primary control for enhanced dynamic response of AC microgrids. *IEEE Transactions on Smart Grid*, 10(3), 3149–3161.

Prodanovic, M. and Green, T. (2003). Control and filter design of three-phase inverters for high power quality grid connection. *IEEE Transactions on Power Electronics*, 18(1), 373–380.

Salton, A.T. (2011). *High Performance Dual-Stage Systems*. VDM Verlag.

Vasiladiotis, M., Christe, A., and Geyer, T. (2019). Model predictive pulse pattern control for modular multilevel converters. *IEEE Transactions on Industrial Electronics*, 66(3), 2423–2431.